Three-Dimensional Reference Interaction Site Model Self-Consistent Field Analysis of Solvent and Substituent Effects on the Absorption Spectra of Brooker's Merocyanine

Yuichi Tanaka, Norio Yoshida,* and Haruyuki Nakano*

Solvent and substituent effects on the absorption spectra of Brooker's merocyanine (BM) are investigated using the three-dimensional reference interaction site model self-consistent field method and time-dependent density functional theory. The $\pi-\pi*$ excitation energies are computed for BM and its derivative 2,6-di-*tert*-butyl (di-*t*-Bu) BM. The behaviors of the computed excitation energies with increasing solvent polarity are in good agreement with those of the corresponding experimental measurements. In addition, analysis of the solute–solvent interaction energies and spatial distribution functions reveals that the effects of the solvent on the absorption spectra are reduced by the steric hindrance of the *t*-Bu groups. Furthermore, from the difference in the solute–solvent interaction energies of BM and di-*t*-Bu BM, it is shown that the effect of the *t*-Bu substituents on the absorption spectrum is greater in high-polarity solvents. © 2015 Wiley Periodicals, Inc.

DOI: 10.1002/jcc.23980

Introduction

Solvatochromism is a phenomenon involving a change in the color of a solution depending on the solvent.[1,2] This phenomenon is now utilized in many fields of chemistry and biology to study the bulk and local polarity in macrosystems; therefore, many experimental and theoretical studies on solvatochromism have been reported to date. The compound 1-methyl-4-[(oxocyclohexadienylidene)ethylidene]-1,4-dihydropyridine, often referred to as Brooker's merocyanine (BM, Fig. 1), is a typical solvatochromic dye and is widely known as a molecule that shows a large solvatochromic shift.[3–7] For instance, the wavelength of the S_1-S_0 transition due to $\pi-\pi*$ excitation is 619.5 nm (2.00 eV) in chloroform and 442.0 nm (2.81 eV) in water. This large shift has been generally understood from the resonance of the zwitterionic (ZW) and neutral (NE) valence bond (VB) structures (Fig. 1).

Figure 2 shows a schematic representation of the energy dependence of the two VB structures on the solvent polarity. The energy of the ZW VB structure largely depends on the solvent polarity because of its polarized nature and decreases with increasing polarity. Conversely, the energy of the NE VB structure is nearly independent of the polarity. The curves for these energies cross in the medium-low polarity region for BM. As a result of the interaction between the two VB structures, the ground and excited states are expressed with superposition of the ZW and NE VB structures. In the low-polarity region, the NE (ZW) VB structure dominates in the ground (excited) state, whereas in the medium to high-polarity region, the ZW (NE) VB structure dominates in the ground (excited) state. In the medium-low polarity region, the two VB structures compete. The dependence of the excitation energy (or absorption wavelength) is qualitatively explained by the difference between the solid lines that show avoided crossing. As a consequence of the avoided crossing, the excitation energy dependence on the polarity is expressed as a downward convex curve.

In the solvatochromism of BM, substituents are known to play an important role. Gruda and Bolduc synthesized several derivatives of BM and obtained their visible absorption spectra in various media.[8] They observed that the absorption energies of the 2,6-di-*tert*-butyl (di-*t*-Bu) derivative were less affected by the solvent polarity than the unsubstituted compound. They also found that the relative intensities of the fine structures were sensitive to the solvent polarity if the substituents were bulky *t*-Bu groups. Catalán et al. obtained the absorption and emission spectra of both di-*t*-Bu BM (Fig. 3) and BM in 28 solvents.[9] They examined the polarity effect on the solvatochromism by blocking the effect of the solvent acidity using the bulky *t*-Bu groups in the ortho position and found that it is very weak and negative. The observed absorption energies of di-*t*-Bu BM in $CHCl_3$ and H_2O were 1.96 and 2.35 eV, respectively, and the solvation shift of di-*t*-Bu BM from $CHCl_3$ to H_2O is much smaller than that of BM. Morley et al. assessed the spectroscopic properties of soluble derivatives of BM both experimentally and theoretically.[10] Their results suggested that the large solvatochromic shift in the visible region for these merocyanines arises because of both dielectric and

Y. Tanaka, N. Yoshida, H. Nakano
Department of Chemistry, Graduate School of Sciences, Kyushu University, Fukuoka, 812-8581, Japan
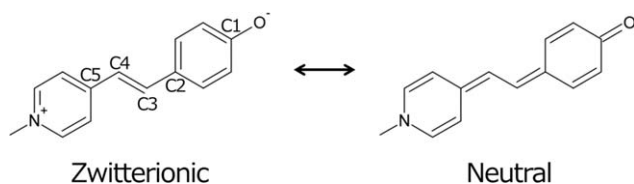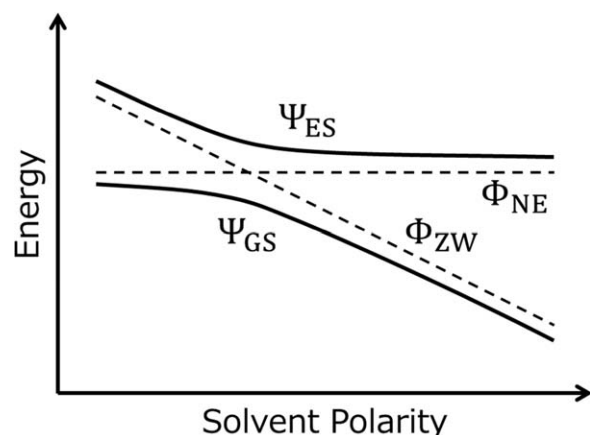*E-mail: noriwo@chem.kyushu-univ.jp or nakano@chem.kyushu-univ.jp*

Figure 1. Resonance structure of BM.

hydrogen bonding effects, and the shifts of the derivatives of BM are larger, because the phenoxide oxygen atom is more exposed to the dielectric field of the solvent and can more readily form hydrogen bonds.

The excitation spectra of BM and its derivatives have also been well-studied theoretically using *ab initio* and semiempirical methods.[11–15] Murugan et al. investigated the intramolecular and solvent shell structures of BM in chloroform and water using the Car–Parrinello hybrid quantum mechanics/molecular mechanics (CP-QM/MM) method.[11] In addition to the solute and solvent structures, they also calculated the absorption spectra using time-dependent density functional theory (TD-DFT) with the Coulomb attenuated B3LYP (CAM-B3LYP) exchange-correlation functional for configurations picked up from the CP molecular dynamics trajectory. The excitation energies in chloroform and water were 2.56 and 2.92 eV, respectively. They concluded that the discrepancy in the experimental and calculated values for the excitation energy in chloroform was attributed to neglecting the dispersion interactions between the solute and the solvent. Adjaye-Mensah et al. obtained absorption spectra and performed excitation energy calculations for a benzofused derivative of BM.[12] They used Truhlar's universal solvation model (SMD),[16] which is a dielectric continuum model, combined with the B3LYP and CAM-B3LYP functionals. The computed excitation energies were correctly ordered for negative solvatochromicity. However, the solvatochromic (blue) shifts were underestimated compared with the experimental values. Wada et al. performed excitation energy calculations for BM in water, methanol, acetonitrile, and dichloromethane using various methods:[13] the polarizable continuum model, the SMD model, the reference interaction site model self-consistent field spatial electron den-

sity distribution (RISM-SCF-SEDD) method,[17] and the mean-field QM/MM method. They obtained qualitatively correct solvent dependence of the solvatochromic shift in the case of the RISM-SCF-SEDD and mean-field QM/MM methods combined with the long-range corrected Becke one-parameter progressive (LC-BOP) exchange-correlation functional.

The theoretical studies mentioned above have clarified the solvent effect on the solvatochromic shifts of BM absorption spectra, but no theoretical studies have yet been conducted to systematically examine both solvent and substituent effects. Therefore, in this study, the solvent and substituent effects on the absorption spectra of BM were investigated using the three-dimensional RISM-SCF (3D-RISM-SCF) method.[18,19] To clarify the substituent effect, a method is necessary that takes into account the interaction between the solute and solvent. In the 3D-RISM-SCF method, the solvent effect, including solute–solvent interaction, is described using the 3D-RISM equation,[20,21] and the electronic structure and the solvation structure (given as a spatial distribution function [SDF]) are obtained simultaneously. Thus, this method is suitable for examining excitation spectra in solution. We previously applied the 3D-RISM-SCF method to the electronic and solvation structures of the chromium hexahydrate trication $[Cr(H_2O)_6]^{3+}$ in water, and the obtained excitation energies that were in good agreement with experimental results.[22] Using the 3D-RISM-SCF method, the absorption spectra of BM and di-*t*-Bu BM in seven solvents were examined. The solute–solvent interaction energies and solvation structures were also investigated to elucidate the origin of the substituent effects on the solvatochromic shifts.
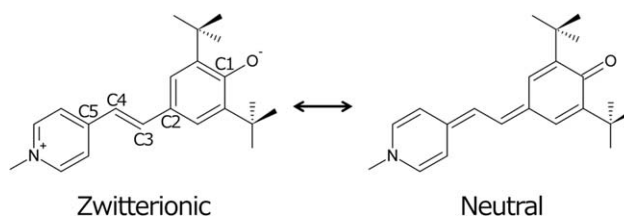
Computational Methods

Excitation energy calculation using the 3D-RISM-SCF method

The 3D-RISM-SCF method and TD-DFT calculations were performed to obtain the vertical excitation energies for BM and di-*t*-Bu BM in solution. The computational scheme is described below.

First, the 3D-RISM-SCF calculation was performed for the ground state of the solute to obtain the SDF $g_\gamma(\mathbf{r})$ of the solvent and the electron density ρ of the solute.

The SDF $g_\gamma(\mathbf{r})$ for the ground state was obtained by solving the 3D-RISM equation combined with the Kovalenko–Hirata (KH) closure:[18]

$$h_\gamma(\mathbf{r}) = c_{\gamma'}(\mathbf{r}) * \left(\omega_{\gamma'\gamma}^{vv}(r) + \rho_{\gamma'} h_{\gamma'\gamma}^{vv}(r) \right), \quad (1)$$

Figure 2. Energy profile of the ground and excited states (Ψ_{GS} and Ψ_{ES}) and the ZW and NE VB structures (Φ_{ZW} and Φ_{NE}) of BM.

Figure 3. Resonance structure of di-*t*-Bu BM.

$$h_\gamma(\mathbf{r}) = \begin{cases} \exp\left(-u_\gamma(\mathbf{r})/k_B T + h_\gamma(\mathbf{r}) - c_\gamma(\mathbf{r})\right) - 1 & \text{for } h_\gamma(\mathbf{r}) \leq 0 \\ -u_\gamma(\mathbf{r})/k_B T + h_\gamma(\mathbf{r}) - c_\gamma(\mathbf{r}) & \text{for } h_\gamma(\mathbf{r}) > 0 \end{cases}.$$

(2)

Here, $h_\gamma(\mathbf{r}) = g_\gamma(\mathbf{r}) - 1$ and $c_\gamma(\mathbf{r})$ are the 3D total and direct correlation functions of the solvent site γ, respectively. The symbols k_B and T represent Boltzmann constant and the absolute temperature, respectively. The functions $\omega_{\gamma\gamma'}^{vv}(r)$ and $h_{\gamma\gamma'}^{vv}(r)$ are the site–site intramolecular and total correlation functions of the solvent, where the superscript "v" denoting the solvent. The $*$ symbol indicates convolution in direct space and summation over repeated site indices. The total correlation function $h_{\gamma\gamma'}^{vv}(r)$ in eq. (1) was set in advance for the 3D-RISM calculation by solving the (1D) RISM equation between the solvent molecules:

$$h_{\gamma\gamma'}^{vv}(r) = \omega_{\gamma\gamma''}^{vv}(r) * c_{\gamma''\gamma'''}^{vv}(r) * \left(\omega_{\gamma'''\gamma'}^{vv}(r) + \rho_{\gamma'''} h_{\gamma'''\gamma'}^{vv}(r)\right), \quad (3)$$

where $c_{\gamma\gamma'}^{vv}(r)$ is the site–site direct correlation function of the solvent.

The electron density ρ in the solute molecule was obtained using the Kohn–Sham (KS) equation:

$$f\phi = \epsilon\phi, \quad (4)$$

where f is the KS operator including the interaction from the solvent molecules, ϵ is the obital energy, and ϕ is the KS orbital.

The electronic density of the solute in the ground state ρ and the distribution of the solvent $g_\gamma(\mathbf{r})$ were determined self-consistently from the 3D-RISM equation set [eqs. (1) and (2)] and the KS equation [eq. (4)]. More details on the 3D-RISM-SCF method can be found elsewhere.[18,19]

After determination of ρ and $g_\gamma(\mathbf{r})$, the vertical excitation energies were computed using the TD-DFT calculations with the electrostatic potential $\hat{V}(\mathbf{r})$ due to the solvent molecules as the external field. The potential $\hat{V}(\mathbf{r})$ is defined by the following equation:

$$\hat{V}(\mathbf{r}) = \begin{cases} 0 & \text{in gas} \\ \sum_{\gamma=1}^{N_v} \rho_\gamma \int d\mathbf{r}' \dfrac{q_\gamma}{|\mathbf{r} - \mathbf{r}'|} g_\gamma(\mathbf{r}') & \text{in solution,} \end{cases}$$

(5)

where N_v is the number of solvent sites, and ρ_γ and q_γ are the number density and point charge of the solvent site γ, respectively.

Computational details

In the DFT and TD-DFT calculations, the LC-BOP exchange-correlation functional[23] and the augmented correlation-consistent polarized valence double-zeta (aug-cc-pVDZ) basis set[24,25] were used unless mentioned. The LC-BOP functional was selected because some excitations involve charge transfer; therefore, long-range correction was crucial in the exchange functional. The LC-BLYP[23] and CAM-B3LYP[26] functionals were also examined to confirm the validity of LC-BOP functional. The details are given in Supporting Information. The aug-cc-

Table 1. Solvent polarity parameters $E_T(30)$ and densities ρ.

Solvent	$E_T(30)$	ρ/molecules Å^{-3} (g cm^{-3})
Gas	27.1	
CCl$_4$	32.4	0.006238 (1.5938)
CHCl$_3$	39.1	0.007497 (1.4867)
(CH$_3$)$_2$CO	42.2	0.008192 (0.7904)
(CH$_3$)$_2$SO	45.1	0.008476 (1.1000)
CH$_3$CN	45.6	0.011383 (0.7762)
CH$_3$OH	55.4	0.014781 (0.7867)
H$_2$O	63.1	0.033316 (0.9970)

pVDZ was used to mainly express the negative charge on the phenoxide oxygen atom.

The molecular structures were optimized in the gas and solution [tetrachloromethane (CCl$_4$), chloroform (CHCl$_3$), acetone ((CH$_3$)$_2$CO), dimethylsulfoxide ((CH$_3$)$_2$SO), acetonitrile (CH$_3$CN), methanol (CH$_3$OH), and water (H$_2$O)] phases. For the optimization calculations, the SMD model proposed by Marenich et al. was used.[16] The parameters of the solvent polarity $E_T(30)$ introduced by Reichardt[1,2] are summarized in Table 1.

In the 3D-RISM calculations, the sum of the Coulomb and Lennard-Jones (LJ) potentials:

$$u_\gamma(\mathbf{r}) = -\sum_{i=1}^{N_e} \int d\mathbf{r}' \frac{|\phi_i(\mathbf{r}')|^2 q_\gamma}{|\mathbf{r} - \mathbf{r}'|} + \sum_{\alpha=1}^{N_u} \frac{Z_\alpha q_\gamma}{|\mathbf{r} - \mathbf{r}_\alpha|} + \sum_{\alpha=1}^{N_u} 4\varepsilon_{\alpha\gamma} \left[\left(\frac{\sigma_{\alpha\gamma}}{|\mathbf{r} - \mathbf{r}_\alpha|}\right)^{12} - \left(\frac{\sigma_{\alpha\gamma}}{|\mathbf{r} - \mathbf{r}_\alpha|}\right)^6 \right],$$

(6)

was chosen as the solute–solvent interaction potential. Here, $\phi_i(\mathbf{r}')$ is the KS molecular orbital, N_e and N_u are the numbers of electrons and solute atoms, α represents the solute atom, and Z_α indicates the charge of the solute atom α. The Lorentz–Berthelot combining rule was applied to the LJ parameters $\sigma_{\alpha\gamma}$ and $\varepsilon_{\alpha\gamma}$:

$$\sigma_{\alpha\gamma} = \frac{\sigma_\alpha + \sigma_\gamma}{2}, \quad (7)$$

$$\varepsilon_{\alpha\gamma} = \sqrt{\varepsilon_\alpha \varepsilon_\gamma}. \quad (8)$$

The LJ parameters and point charges are listed in Supporting Information. The optimized potentials for liquid simulations (OPLS) parameters were used for BM, di-t-Bu BM, and the solvents, except for H$_2$O.[27–31] The parameters of H$_2$O were taken from the extended simple point charge model (SPC/E).[32] The LJ parameters of the hydrogen atoms of H$_2$O and the hydroxyl group of CH$_3$OH were $\sigma = 0.4$ Å and $\varepsilon = 0.046$ kcal mol^{-1}. The densities of the solvents are summarized in Table 1. The temperature was 298.15 K. Rectangular grid boxes, the axes of which had 256 grid points with a spacing of 0.25 Å, were used in the 3D-RISM calculations.

All the calculations were performed using a modified version[33] of the GAMESS program package.[34]

Results and Discussion

Electronic structures of the low-lying excited states

Prior to discussing the solvent and substituent effects, some of the low-lying excited states of BM and di-t-Bu BM computed

Table 2. Excitation energies, oscillator strengths, and weights of configurations for the low-lying excited states of BM and di-*t*-Bu BM in the gas phase.[a]

State	Configuration	BM	di-*t*-Bu BM
S_1		2.95 eV (420.3 nm) $f = 1.478$	2.86 eV (433.8 nm) $f = 1.527$
	HOMO → LUMO	95.0%	95.2%
S_2		3.45 eV (359.5 nm) $f = 0.000$	3.38 eV (366.4 nm) $f = 0.000$
	HOMO−1 → LUMO	70.9%	71.5%
S_3		3.65 eV (339.8 nm) $f = 0.054$	3.62 eV (342.6 nm) $f = 0.050$
	HOMO → LUMO+4	52.2%	38.7%
	HOMO → LUMO+5	31.5%	33.3%
S_4		4.43 eV (279.8 nm) $f = 0.007$	4.37 eV (283.8 nm) $f = 0.008$
	HOMO → LUMO+1	48.8%	50.3%
	HOMO → LUMO+3	33.6%	29.2%

[a] Only configurations with weights greater than 20% are shown.

using the TD-DFT method were shortly described. Table 2 lists the excitation energies and main configurations of the four low-lying singlet excited states of both molecules in the gas phase. In these molecules, the lowest excited state (S_1) is located in the visible-light region, whereas the other three excited states are in the near ultraviolet region. Figure 4 shows the KS molecular orbitals from the second highest occupied molecular orbital (HOMO−1) to the sixth lowest unoccupied molecular orbital (LUMO+5), which, except for LUMO+2, are involved in the four excited states in Table 2.

The shapes of the corresponding orbitals of BM and di-*t*-Bu BM are very similar, except for HOMO−1. The second HOMO (HOMO−1) is an n-type orbital storing the lone-pair electrons on the phenoxide oxygen, though that of di-*t*-Bu BM has a certain amount of the electron distribution on the *t*-Bu groups in addition to the phenoxide oxygen. The HOMO and LUMO are π-type orbitals that are delocalized over the entire molecule. The fifth and sixth LUMOs (LUMO+4 and LUMO+5) are also π-type orbitals. However, unlike the HOMO and LUMO, they are almost completely localized on the pyridinium ring. The remaining second, third, and fourth LUMOs (LUMO+1, LUMO+2, and LUMO+3) are σ-type orbitals.

The S_1 states for both BM and di-*t*-Bu BM involve the HOMO (π) to LUMO (π*) excited state and each is almost completely expressed by a single configuration (the weight of the HOMO–LUMO configuration is approximately 95% for both molecules) with a considerable oscillator strength ($f = 1.478$ and 1.527 for BM and di-*t*-Bu BM, respectively). The second excited state (S_2) in each compound is the HOMO−1 (n) to LUMO (π*) excited state. However, the weight of the main configuration is comparatively smaller (about 70%) than that of S_1, and the oscillator strength for this excitation is approximately zero for both molecules. The third and fourth excited states (S_3 and S_4) are mainly due to the HOMO to LUMO+4 and HOMO to LUMO+1 excitations, respectively, and the oscillator strengths for these excited states are rather small compared with that of S_1 for both compounds. As mentioned above, only S_1 in both BM and di-*t*-Bu BM is in the visible-light region and has a large oscillator strength, indicating that it is responsible for the solvatochromic color change. Hereafter, only S_1 is discussed.

Note that the orbital shapes, orbital energies, excitation energies, and oscillator strengths of S_1 for BM and di-*t*-Bu BM are very similar in the gas phase. This similarity implies that the origin of the substituent effect is not due to a change in the electronic structure but due to the change in the interaction between the solute molecule and the solvents.

Solvent dependence of the excitation energy

Next, the solvent effects on the excitation energy for BM and di-*t*-Bu BM were evaluated.

Figure 5 shows the computed and experimental π–π* excitation energies of BM and di-*t*-Bu BM plotted as a function of the $E_T(30)$ values. Note that the computed results for BM in cyclohexane ($E_T(30) = 30.9$) are not shown because convergence of the RISM equation [eq. (3)] for this solvent system could not be achieved. As the solvent polarity increased, the experimental excitation energy of BM initially decreased, reaching a minimum value of 2.00 eV, at $E_T(30) = 39.1$ (CHCl$_3$), and then increased to 2.81 eV. Conversely, the experimental excitation energy of di-*t*-Bu BM increased monotonically in the range of the available experimental data, and all of the values were lower than the corresponding values of BM.

The computed excitation energy has minimum values for both BM (2.73 eV at $E_T(30) = 39.1$) and di-*t*-Bu BM (2.64 eV at $E_T(30) = 42.2$). The computed values of both molecules exhibited a behavior similar to the corresponding experimental values but were comparatively overestimated. A key difference from the experimental results was observed for the excitation energies in (CH$_3$)$_2$SO ($E_T(30) = 45.1$) and CH$_3$CN ($E_T(30) = 45.6$); the order was reversed for both BM and di-*t*-Bu BM. In general, the computed values showed relatively better agreement to the experiment results for protic solvents (CH$_3$OH and H$_2$O). This tendency has also been reported by Wada et al.,[13] who examined the absorption spectrum of BM using the continuum model, QM/MM, and RISM-SCF-SEDD methods combined with TD-DFT calculations. These results suggest that the tendency is not specific in the 3D-RISM-SCF method, but common to several solvent models.

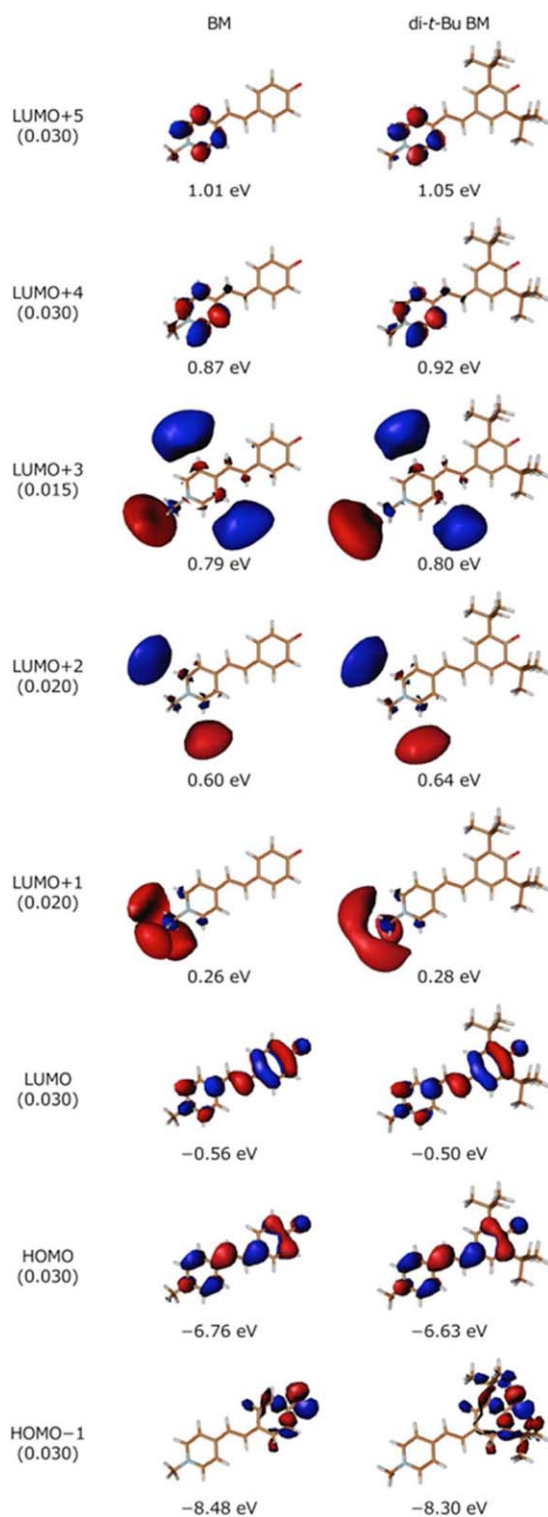The qualitative agreement between the experimental and calculated results for the solvent dependence on the excitation

Figure 4. Isosurface plots for selected KS molecular orbitals of BM and di-*t*-Bu BM in the gas phase and their orbital energies (The numbers in the parentheses are isovalues.).

energy allowed us to discuss the substituent effects on the solvatochromic shift using the 3D-RISM-SCF method.

The fact that the excitation energy reaches a minimum at approximately $E_T(30) = 40$ can be explained by the change in the dipole moments of the solute molecules. In Table 3, the

dipole moments of BM and di-*t*-Bu BM in both ground and excited states in different solvents are summarized. In the gas phase and low-polarity solution phases, the dipole moments in the ground state are less than those in the excited state, whereas in high-polarity solutions, the dipole moments in the ground state are larger than those in the excited state. These results imply that the solvent stabilizes the excited state more than the ground state in the low-polarity solution; hence, the excitation energy decreases with increasing solvent polarity. Conversely, in high-polarity solutions, the ground state is more stabilized than the excited state; thus, the excitation energy increases. This behavior of the dipole moment is in agreement with the VB picture shown in Figure 2. The state with a large (small) ZW VB structure in its wave function has a large (small) dipole moment, which corresponds to the excited (ground) state in the low-polarity region and the ground (excited) state in the medium to high-polarity region.

The bond order analysis also supports the VB picture. Table 4 shows Mulliken bond orders of the O—C1, C2—C3, C3—C4, and C4—C5 bonds (the labels of atoms are shown in Figures 1 and 3). Here, to evaluate the bond order properly, we used the cc-pVDZ basis set (no diffuse functions) with the same molecular structures and solvation structures obtained with the aug-cc-pVDZ basis set. The bond orders of the O—C1, C2—C3, and C4—C5 bonds decrease with increasing solvent polarity, whereas that of the C3—C4 bond increases. This result indicates increasing contribution of the ZW VB structure with increasing solvent polarity in the ground state.

Substituent effects on the solvent dependence of the excitation energy

To discuss the substituent effects on the excitation energy, the difference in excitation energies of BM and di-*t*-Bu BM was investigated.

Figure 6 shows the difference, δE:

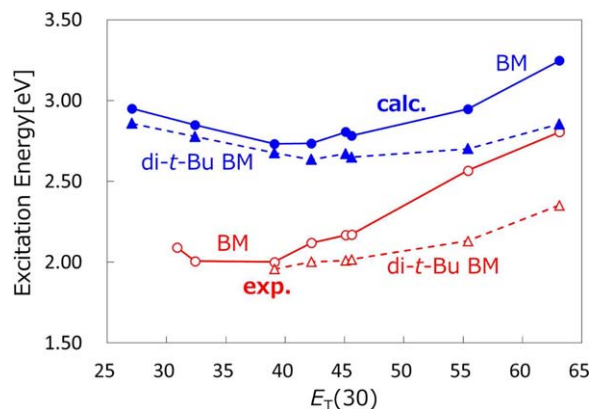$$\delta E = E^{BM} - E^{\text{di-}t\text{-Bu BM}}, \tag{9}$$

Figure 5. BM (circles, solid lines) and di-*t*-Bu BM (triangles, dashed lines) π–π^* excitation energies as a function of the $E_T(30)$ values. The red ($\bigcirc$, $\triangle$) and blue ($\bullet$, $\blacktriangle$) lines indicate the experimental and computational results, respectively. The experimental values were taken from Refs. [4] and [9] for BM and di-*t*-Bu BM, respectively. [Color figure can be viewed in the online issue, which is available at wileyonlinelibrary.com.]

Table 3. Dipole moments for the solute molecules in different solvents (debye).

Solvent	BM		di-t-Bu BM	
	S_0	S_1	S_0	S_1
Gas	15.1	17.7	13.5	16.2
CCl$_4$	16.4	18.1	14.7	16.5
CHCl$_3$	21.4	21.2	18.5	19.0
(CH$_3$)$_2$CO	28.0	24.9	24.6	22.5
(CH$_3$)$_2$SO	30.6	26.4	27.1	24.1
CH$_3$CN	30.1	26.1	26.2	23.4
CH$_3$OH	35.2	28.7	29.0	25.1
H$_2$O	40.1	32.6	33.9	28.2

Figure 6. Experimental (○, red line) and calculated (3D-RISM-SCF method; ●, blue line) differences in the excitation energies for BM and di-t-Bu BM, δE, plotted as a function of $E_T(30)$. The experimental values were obtained from Refs. [4] and [9]. [Color figure can be viewed in the online issue, which is available at wileyonlinelibrary.com.]

plotted against $E_T(30)$. Here, E^{BM} and $E^{di\text{-}t\text{-}Bu\ BM}$ denote the excitation energies of BM and di-t-Bu BM, respectively. In this figure, it can be seen that both the experimental and calculated results exhibited similar tendencies when $E_T(30) \geq 39.1$; that is, δE was always positive and increased with the solvent polarity, except when $E_T(30) = 45.6$. The computed results were in good agreement with the experimental values in the range from $E_T(30) = 39.1$ to 45.6, with deviations less than 0.03 eV. Conversely, relatively large deviations were observed for the protic solvents (0.20 eV for CH$_3$OH and 0.06 eV for H$_2$O). For the low-polarity solvents, the computed values for δE decreased with increasing solvent polarity, but no experimental values were available for comparison.

To gain more insight into the substituent effects on the solvent dependences, two solvents were investigated further. Table 5 lists the computed excitation energies for BM and di-t-Bu BM in the gas phase and in CHCl$_3$ and H$_2$O solutions, along with the differences in the values for the gas and corresponding solution phases. The data for the other solvents are provided in Supporting Information. The difference in the excitation energy for a compound in the gas and solution phase provides information on the magnitude of the solvent

Table 4. Mulliken bond orders of the solute molecules calculated with the cc-pVDZ basis set.[a]

Solvent	O—C1	C2—C3	C3—C4	C4—C5
		BM		
Gas	2.16	1.58	1.20	1.57
CCl$_4$	2.14	1.55	1.24	1.53
CHCl$_3$	2.08	1.46	1.32	1.44
(CH$_3$)$_2$CO	2.06	1.36	1.43	1.33
(CH$_3$)$_2$SO	2.05	1.32	1.47	1.30
CH$_3$CN	2.04	1.33	1.47	1.31
CH$_3$OH	1.89	1.25	1.55	1.25
H$_2$O	1.75	1.20	1.62	1.20
		di-t-Bu BM		
Gas	2.07	1.57	1.19	1.56
CCl$_4$	2.06	1.54	1.22	1.53
CHCl$_3$	2.02	1.48	1.28	1.46
(CH$_3$)$_2$CO	1.97	1.39	1.38	1.36
(CH$_3$)$_2$SO	1.95	1.36	1.42	1.33
CH$_3$CN	1.96	1.37	1.41	1.34
CH$_3$OH	1.87	1.33	1.45	1.31
H$_2$O	1.76	1.27	1.52	1.26

[a] The labels of the atoms are shown in Figures 1 and 3.
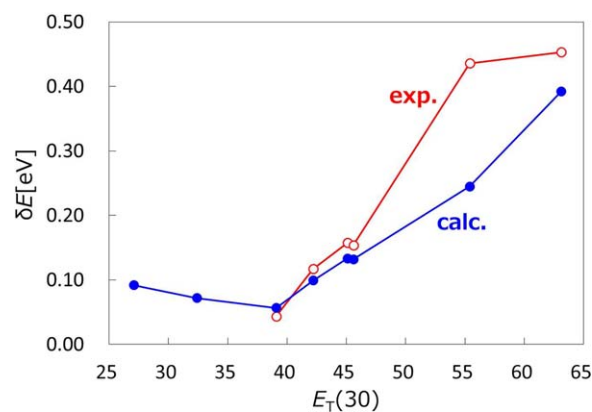
effect. The computed data in Table 5 clearly indicate that the solvent effects on the excitation energy are weakened by the presence of the two ortho t-Bu groups.

To further analyze the solvent effects due to substitution, the solute–solvent interaction energies were examined. Figure 7 shows the interaction energy, E_O^{int}, between the phenoxide oxygen atom of the solute and the solvent molecules around the solute molecule in the ground state, where E_O^{int} is defined by:

$$E_O^{int} = \sum_{\gamma=1}^{N_v} \rho_\gamma \int d\mathbf{r} g_\gamma(\mathbf{r}) \left\{ \frac{q_O q_\gamma}{|\mathbf{r}-\mathbf{r}_O|} + 4\varepsilon_{O\gamma} \left[\left(\frac{\sigma_{O\gamma}}{|\mathbf{r}-\mathbf{r}_O|} \right)^{12} - \left(\frac{\sigma_{O\gamma}}{|\mathbf{r}-\mathbf{r}_O|} \right)^6 \right] \right\}. \tag{10}$$

The first and second terms in the curly brackets are the Coulomb and LJ interaction terms, respectively, and q_O is the effective partial charge of the phenoxide oxygen atom, which was determined to reproduce the electrostatic potential around the solute molecule using least-squares fitting. The detailed values of the interaction energies in the ground and excited states are summarized in Supporting Information. In Figure 7, it can be seen that the absolute value of E_O^{int}, $|E_O^{int}|$, increases as the solvent polarity increases, and $|E_O^{int}|$ for di-t-Bu BM is smaller than that of BM in all of the solvents. In addition, the difference in E_O^{int} increases as the solvent polarity increases. These results suggest the substituent effects of the t-Bu groups on E_O^{int} are greater in more polar solvents.

Because E_O^{int} is dependent on the solvent distribution, SDF, and the solute point charge on the phenoxide oxygen, q_O [see

Table 5. Excitation energies for BM and di-t-Bu BM in the gas phase and H$_2$O, and CHCl$_3$ solutions (eV).[a]

Solvent	BM	di-t-Bu BM
Gas	2.95 (0.00)	2.86 (0.00)
CHCl$_3$	2.73 (−0.22)	2.68 (−0.18)
H$_2$O	3.25 (0.30)	2.85 (−0.01)

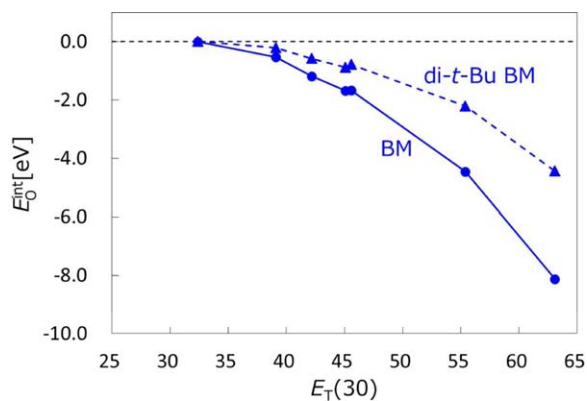[a] Numbers in parentheses indicate the difference from the corresponding gas phase values.

Figure 7. Calculated interaction energies E_O^{int} for BM (●, solid line) and di-*t*-Bu BM (▲, dashed line) plotted as a function of $E_T(30)$. [Color figure can be viewed in the online issue, which is available at wileyonlinelibrary.com.]

Figure 9. RDFs around the phenoxide oxygen atom of BM (solid lines) and di-*t*-Bu BM (dashed lines) in H_2O (oxygen: red thin lines, hydrogen: black thick lines). [Color figure can be viewed in the online issue, which is available at wileyonlinelibrary.com.]

(10)], further information on the substituent effects can be obtained by evaluating the SDFs and q_O values for different solvents. Figure 8 shows the SDFs around BM and di-*t*-Bu BM for H_2O (see Supporting Information for the SDFs of the other solvents). A hydrogen atom of a solvent H_2O molecule has a conspicuous distribution in the vicinity of the phenoxide oxygen of the BM, and the distribution of the oxygen of the solvent H_2O molecule is outside the hydrogen distribution. These distributions indicate that a hydrogen atom in a solvent H_2O molecule forms a hydrogen bond with the phenoxide oxygen. Conversely, in the case of di-*t*-Bu BM, while the distribution of a solvent hydrogen atom can also be found around the phenoxide oxygen, the distributed region is narrower than that of BM because of the steric hindrance of the *t*-Bu groups. Additional distributions of hydrogen are found at the upper and
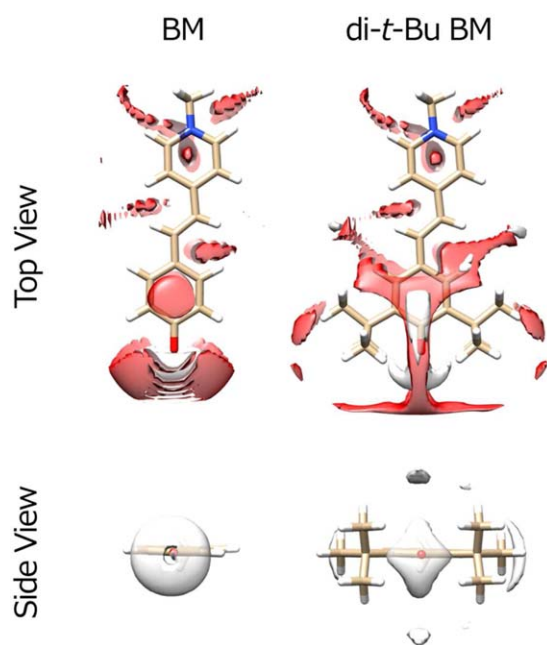
lower sides of the C=O group in di-*t*-Bu BM, which are not observed in the case of BM; however, these distributions do not strongly affect E_O^{int}, because they are far from the phenoxide oxygen.

Figure 9 shows the radial distribution functions (RDFs, $g_{O\gamma}(r)$) of H_2O around the phenoxide oxygen atoms in BM and di-*t*-Bu BM obtained via angular averaging of the SDFs, and Figure 10 shows the coordination numbers, $N_{O\gamma}(r)$, obtained via radial integration of the RDFs:

$$g_{O\gamma}(r) = g_\gamma(r, \mathbf{r}_O) = \frac{1}{4\pi}\int d\hat{\mathbf{r}} g_\gamma(\mathbf{r}_O + \mathbf{r}), \quad (11)$$

$$N_{O\gamma}(r) = 4\pi\rho_\gamma \int_0^r dr' r'^2 g_{O\gamma}(r'), \quad (12)$$

where $\hat{\mathbf{r}}$ is a direction of vector $\mathbf{r}$, and $\mathbf{r}_O$ is the center for the angular averaging placed at the phenoxide oxygen atom of the solute molecule. In Figure 9, the first peak of di-*t*-Bu BM is lower than that of BM. This feature of the RDFs is attributed to the steric hindrance of the *t*-Bu groups and was observed in all of the solvents (see Supporting Information). As a result

Figure 8. Isosurface plots of the SDFs around BM and di-*t*-Bu BM in H_2O (O: red, isovalue = 3.0; H: white, isovalue = 2.0). Only the hydrogen distributions are plotted in the side view for simplicity.
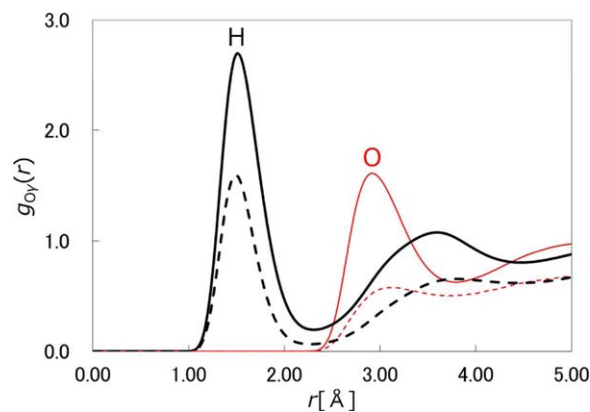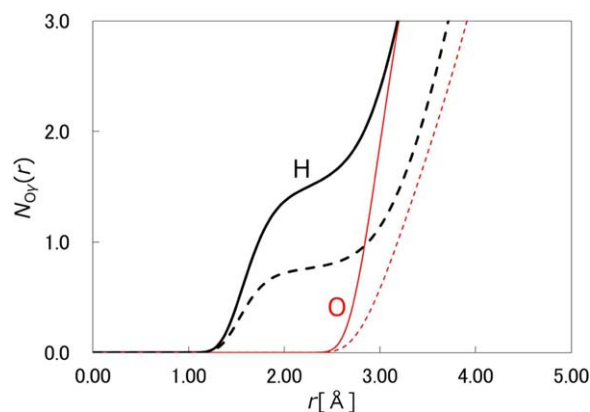

Figure 10. Coordination number $N_{O\gamma}(r)$ around the phenoxide oxygen atom of BM (solid lines) and di-*t*-Bu BM (dashed lines) in H_2O (oxygen: red thin lines, hydrogen: black thick lines). [Color figure can be viewed in the online issue, which is available at wileyonlinelibrary.com.]

Table 6. Effective charges of the phenoxide oxygen atom of the solute q_O in different solvents in the ground state (atomic unit).[a]

Solvent	BM	di-t-Bu BM
Gas	−0.6408 (0.0000)	−0.5137 (0.0000)
CCl$_4$	−0.6512 (−0.0104)	−0.5225 (−0.0088)
CHCl$_3$	−0.7149 (−0.0741)	−0.5531 (−0.0394)
(CH$_3$)$_2$CO	−0.7746 (−0.1338)	−0.5930 (−0.0793)
(CH$_3$)$_2$SO	−0.7997 (−0.1589)	−0.6106 (−0.0969)
CH$_3$CN	−0.8088 (−0.1680)	−0.6091 (−0.0954)
CH$_3$OH	−0.9751 (−0.3343)	−0.7443 (−0.2306)
H$_2$O	−1.1369 (−0.4961)	−0.9050 (−0.3913)

[a] Numbers in parentheses indicate the difference in q_O from the gas phase values.

of the lowering of the RDFs, the coordination numbers of di-t-Bu BM in Figure 10 are less than those of BM. The smaller number of solvent molecules in the vicinity of the phenoxide oxygen because of the steric hindrance of the t-Bu groups is the reason for the smaller $|E_O^{int}|$ value of di-t-Bu BM compared with that of BM.

Finally, the effective point charges on the phenoxide oxygen of the solute molecule (q_O) in different solvents are listed in Table 6. The q_O values for the excited state are available in Supporting Information. As can be seen in Table 6, q_O monotonically increases with increasing solvent polarity, except for di-t-Bu BM in CH$_3$CN. Notably, the enhancement of q_O with increasing solvent polarity is less for di-t-Bu BM than BM. The reduced enhancement results from the reduced solvent distribution because of the steric hindrance, as discussed above, and contributes to the smaller $|E_O^{int}|$ values of di-t-Bu BM compared with those of BM.

Conclusions

In this article, we investigated the solvent and substituent effects on the absorption spectra of BM and di-t-Bu BM using the 3D-RISM-SCF method. The computed results qualitatively reproduced the experimental data, and detailed analysis on the computed results clarified the origin of the substituent effect, which is mainly the steric effect of the bulky t-Bu groups.

In summary, the 3D-RISM-SCF analysis revealed the following aspects:

1. The excitation energy does not vary monotonically with the solvent polarity. It initially decreases to reach a minimum value, and then increases with the solvent polarity. This behavior can be explained by the difference in the solute dipole moments in the ground and excited states.
2. The solvent effects on the excitation energy are weakened by substitution. The number of coordinated solvent molecules calculated on the basis of the SDFs decreases because of the steric hindrance of the t-Bu groups, which reduces the solvent effects on the absorption spectra.
3. Greater substituent effects on the excitation energy are observed in higher-polarity solvents. The difference in

the solute–solvent interaction energy of BM and di-t-Bu BM increases with the solvent polarity.

This study demonstrated that the 3D-RISM-SCF method is effective for qualitatively reproducing the solvent and substituent effects on the absorption spectra of solvated molecules. We, therefore, expect that this method will be useful for the theoretical molecular design and color tuning of chromophores.

[1] C. Reichardt, T. Welton, Solvents and Solvent Effects in Organic Chemistry, 4th ed.; Wiley-VCH: Weinheim, **2011**.
[2] C. Reichardt, *Chem. Rev.* **1994**, *94*, 2319.
[3] L. G. S. Brooker, G. H. Keyes, D. W. Heseltine, *J. Am. Chem. Soc.* **1951**, *73*, 5350.
[4] P. Jacques, *J. Phys. Chem.* **1986**, *90*, 5535.
[5] M. Tsukada, Y. Mineo, K. Itoh, *J. Phys. Chem.* **1989**, *93*, 7989.
[6] I. Baraldi, G. Brancolini, F. Momicchioli, G. Ponterini, D. Vanossi, *Chem. Phys.* **2003**, *288*, 309.
[7] S. T. Abdel-Halim, M. K. Awad, *J. Mol. Struct.* **2005**, *754*, 16.
[8] I. Gruda, F. Bolduc, *J. Org. Chem.* **1984**, *49*, 3300.
[9] J. Catalán, E. Mena, W. Meutermans, J. Elguero, *J. Phys. Chem.* **1992**, *96*, 3615.
[10] J. O. Morley, R. M. Morley, R. Docherty, M. H. Charlton, *J. Am. Chem. Soc.* **1997**, *119*, 10192.
[11] N. A. Murugan, J. Kongsted, Z. Rinkevicius, K. Aidas, H. Ågren, *J. Phys. Chem. B* **2010**, *114*, 13349.
[12] E. Adjaye-Mensah, W. G. Gonzalez, J. Miksovska, J. N. Wilson, *J. Phys. Chem. A* **2012**, *116*, 12470.
[13] T. Wada, H. Nakano, H. Sato, *J. Chem. Theory Comput.* **2014**, *10*, 4535.
[14] A. Botrel, A. Le Beuze, P. Jacques, H. Strub, *J. Chem. Soc., Faraday Trans. 2* **1984**, *80*, 1235.
[15] V. Luzhkov, A. Warshel, *J. Am. Chem. Soc.* **1991**, *113*, 4491.
[16] A. V. Marenich, C. J. Cramer, D. G. Truhlar, *J. Phys. Chem. B* **2009**, *113*, 6378.
[17] D. Yokogawa, H. Sato, S. Sakaki, *J. Chem. Phys.* **2007**, *126*, 244504.
[18] A. Kovalenko, F. Hirata, *J. Chem. Phys.* **1999**, *110*, 10095.
[19] H. Sato, A. Kovalenko, F. Hirata, *J. Chem. Phys.* **2000**, *112*, 9463.
[20] D. Beglov, B. Roux, *J. Phys. Chem. B* **1997**, *101*, 7821.
[21] A. Kovalenko, F. Hirata, *Chem. Phys. Lett.* **1998**, *290*, 237.
[22] S. Fujishige, Y. Kawashima, N. Yoshida, H. Nakano, *J. Phys. Chem. A* **2013**, *117*, 8314.
[23] H. Iikura, T. Tsuneda, T. Yanai, K. Hirao, *J. Chem. Phys.* **2001**, *115*, 3540.
[24] T. H. Dunning, Jr., *J. Chem. Phys.* **1989**, *90*, 1007.
[25] R. A. Kendall, T. H. Dunning, Jr., R. J. Harrison, *J. Chem. Phys.* **1992**, *96*, 6796.
[26] T. Yanai, D. P. Tew, N. C. Handy, *Chem. Phys. Lett.* **2004**, *393*, 51.

[27] W. L. Jorgensen, D. S. Maxwell, J. Tirado-Rives, *J. Am Chem. Soc.* **1996**, *118*, 11225.

[28] E. M. Duffy, D. L. Severance, W. L. Jorgensen, *J. Am. Chem. Soc.* **1992**, *114*, 7535.

[29] W. L. Jorgensen, J. M. Briggs, M. L. Contreras, *J. Phys. Chem.* **1990**, *94*, 1683.

[30] H. Liu, F. Müller-Plathe, W. F. van Gunsteren, *J. Am. Chem. Soc.* **1995**, *117*, 4363.

[31] W. L. Jorgensen, J. M. Briggs, *Mol. Phys.* **1988**, *63*, 547.

[32] H. J. C. Berendsen, J. R. Grigera, T. P. Straatsma, *J. Phys. Chem.* **1987**, *91*, 6269.

[33] N. Yoshida, F. Hirata, *J. Comput. Chem.* **2006**, *27*, 453.

[34] M. W. Schmidt, K. K. Baldridge, J. A. Boatz, S. T. Elbert, M. S. Gordon, J. H. Jensen, S. Koseki, N. Matsunaga, K. A. Nguyen, S. Su, T. L. Windus, M. Dupuis, J. A. Montgomery, Jr., *J. Comput. Chem.* **1993**, *14*, 1347.